ChemComm

Accepted Manuscript

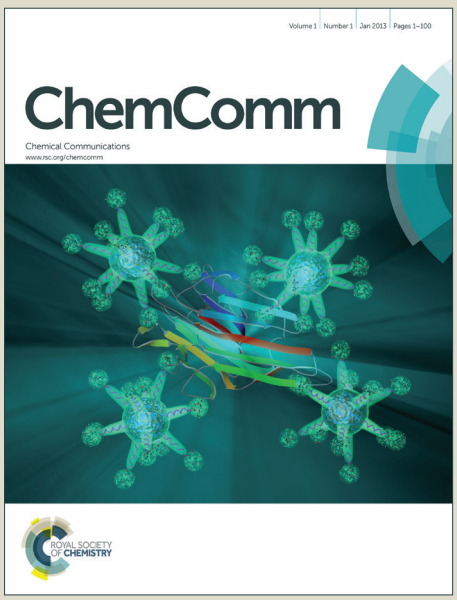

ROYAL SOCIETY OF CHEMISTRY

www.rsc.org/chemcomm

Cite this: DOI: 10.1039/c0xx00000x

www.rsc.org/xxxxxx

Communication

Enhanced Charge-Discharge Properties of SnO_2 Nanocrystallites in Confined Carbon Nanospace

Shinji Oro, Koki Urita and Isamu Moriguchi*

Received (in XXX, XXX) Xth XXXXXXXXX 20XX, Accepted Xth XXXXXXXXX 20XX
DOI: 10.1039/b000000x

Almost perfect embedding of SnO_2 nanocrystallites in carbon nanopores was achieved by *in situ* synthesis using vaporized $SnCl_2$ and silica opal-derived nanoporous carbons. The reversibility of SnO_2-Sn conversion and Sn-Li alloying/de-alloying reactions was greatly enhanced by the confinement in regulated carbon nanospace.

Much research work has been devoted to the development of energy storage devices with both high energy and high power densities due to expected demand for power-grid applications as well as power sources of electric and/or hybrid electric vehicle. Lithium-ion secondary batteries (LIBs) are attractive power storage devices, but they still need to be further improved for the power use. Enhancement of capacities and cycleability of electrode materials is one of the tactics to improve the LIB performance. With respect to the LIB anode materials, SnO_2-based materials have been studied as a candidate of large capacity anode alternative to the present graphite or carbon anode. However, the electrochemical reactions of SnO_2 with Li ions, which are composed of following reactions (1) and (2), are generally irreversible, and thus cause severe capacity fading during cycling.

Conversion reactions: $SnO_2 + 4\,Li^+ + 4\,e^- \leftrightarrow Sn + 2\,Li_2O$ (1)

Alloying/de-alloying reactions: $Sn + x\,Li^+ + x\,e^- \leftrightarrow Li_xSn$ (2)

Some researchers have tried to overcome the problem from the approaches of down-sizing of SnO_2 particles[1-5] and controlling the morphology of SnO_2 such as nanowires,[6] nanotubes[7,8] and nanospheres.[9-12] Some of them succeeded in yielding relatively high initial capacities, but the capacity retention was not improved enough due to cracking and crumbling in the SnO_2-integrated electrodes caused by the volume change during Li insertion and extraction. Nanocomposites of SnO_2 and carbon nanomaterials such as mesoporous carbons,[13-15] carbon nanotubes[16,17] and graphene sheets[18-20] were effective to suppress the mechanical degradation and showed high capacities and a cycleability improved to some extent. The reported charge-discharge capacities of nanocomposites are including electric double layer capacities and/or Li intercalation/de-intercalation capacities of graphite phase, thus it is unclear how much the electrochemical reactions of SnO_2 with Li ions contributed to the total capacities and the capacity retentions. In order to achieve high performance of SnO_2 electrode materials, it is essentially important to clarify the reversibility of electrochemical reactions of SnO_2 with Li ions and which structure is suitable for improving the performance.

Since the reported nanocomposites have heterogeneous structures where SnO_2 nanoparticles are incorporated in irregular interspace and inner pores of carbon nanomaterials and also are deposited on the outer surfaces of them, it is difficult to evaluate exactly the SnO_2 reactions affected significantly by the reaction space. In the present study, we have succeeded in almost perfect embedding of SnO_2 nanocrystallites in the regulated carbon nanopores of ordered porous carbons for the first time, and have evaluated the reversibility of their electrochemical reactions. It is disclosed that the reversibility of charge-discharge reactions of SnO_2 is greatly enhanced in the confined carbon nanospace.

Embedding of SnO_2 nanocrystallites into nanopores of porous carbons was carried out by following two methods: [1] mixing of a nanoporous carbon with a SnO_2 sol in a solution, [2] introduction of $SnCl_2$ vapor and conversion into SnO_2 in the nanopores of nanoporous carbons. A nanoporous carbon with an average pore diameter of 120 nm, 45 nm or 18 nm, which was obtained by a silica opal template process as previously reported,[21] was used for the above syntheses. Hereafter the porous carbon and the SnO_2-embedded nanoporous carbon composites obtained by [1] and [2] methods are denoted as C*X*, SnO_2/C*X*-sol and SnO_2/C*X*-vap, respectively, where *X* indicates the average carbon pore size in nm. SnO_2/C120-sol was obtained by mixing a $SnO_2 \cdot nH_2O$ sol and C120 with the weight ratio of $SnO_2 \cdot nH_2O$/C120 = 85/15 in ethanol under a sonication for 6 h, followed by a filtration and a heating at 120 °C for 2 h. SnO_2/C*X*-vap was synthesized by heating a mixture of $SnCl_2$ and C*X* ($SnCl_2$ /C*X* = 85/15 by weight) in a sealed tube at 320 °C for 24 h, and then washing with pure water and drying in *vacuo*. SnO_2 powder was also synthesized by heating a $SnO_2 \cdot nH_2O$ sol in an O_2 atmosphere (see experimental details in the ESI†).

The production of rutile-type SnO_2 crystallites was confirmed by X-ray diffraction (XRD) measurements for all the samples (Fig. S1, ESI†). The primary crystallite size was estimated to be ca. 3 nm from the full width at half-maximum (FWHM) of the (110) XRD peak using the Scherrer equation. Table 1 shows structural parameters of SnO_2 contents (W_{SnO2}), primary crystallite size of SnO_2 (d), specific surface areas (S_a) and specific pore volumes (V_p) of samples, as well as weighted average values of S_a ($S_{a,w}$) and V_p ($V_{p,w}$) which are calculated under the assumption of a simple mixing of C*X* and SnO_2 nanocrystallites

Table 1 Structural parameters of the samples

Samples	W_{SnO2} (wt%)	d (nm)	S_a (m^2/g)	$S_{a,w}$ (m^2/g)	V_p (cm^3/g)	$V_{p,w}$ (cm^3/g)
SnO_2/C120-vap	74	3.2	258	517	0.23	0.38
SnO_2/C120-sol	66	3.0	265	588	0.35	0.50
SnO_2/C45-vap	62	2.4	379	602	1.42	1.72
SnO_2/C18-vap	56	3.3	575	700	2.04	2.26
C120	–	–	1174	–	1.47	–
C45	–	–	1093	–	4.53	–
C18	–	–	1229	–	5.15	–

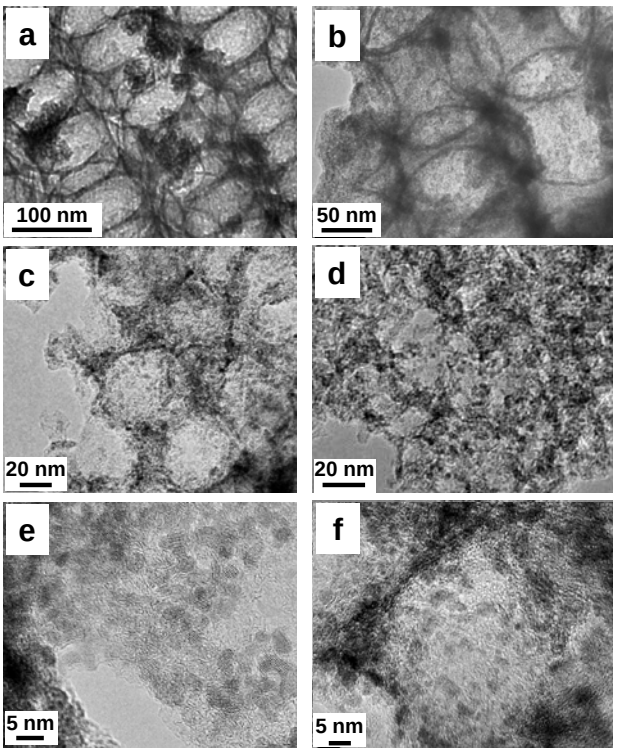

Fig. 1 TEM images of (a) SnO_2/C120-sol, (b) SnO_2/C120-vap, (c) SnO_2/C45-vap, (d) SnO_2/C18-vap, (e) the inner pore of SnO_2/C120-vap, and (f) the inner pore of SnO_2/C45-vap

with the primary crystallite size. The SnO_2 content of SnO_2/C*X*-vap samples determined by thermogravimetry (TG) was 56 to 74 wt%, which corresponds to 68 to 90% conversion of $SnCl_2$ mixed with C*X*. The S_a and V_p values of SnO_2/C*X* samples were smaller than the values of $S_{a,w}$ and $V_{p,w}$, suggesting that SnO_2 nanocrystallites were produced preferentially in carbon nanopores. It was actually observed by transmission electron microscopy (TEM) that SnO_2 nanocrystallites with the size of ca. 3 nm were deposited in nanopores of porous carbons for SnO_2/C*X*-vap samples (Fig. 1). There were no agglomerated SnO_2 particles outside of porous carbons as far as we observed throughout. Porous surface without large agglomerated particles was also confirmed for SnO_2/C45-vap as a representative example by scanning electron microscopy (SEM) (Fig. S2, ESI†). If all of the SnO_2 nanocrystallites are located in the carbon nanopores, the wt% of SnO_2 in SnO_2/C*X*-vap samples ($W_{SnO2,\ calc}$) can be calculated by using the following equations (3) and (4):

$$W_{SnO2,\ calc} = \frac{100x}{1+x} \qquad (3)$$

$$V_{comp} = \frac{V_c - x/\rho}{1+x} \qquad (4)$$

where x is gram of SnO_2 per 1g of carbon in SnO_2/C*X*-vap, V_{comp} and V_c are specific pore volume of the SnO_2/C*X*-vap and the original C*X*, and ρ is the density of SnO_2 crystal (6.95 cm^3 g^{-1}),[22] respectively. The calculated $W_{SnO2,calc}$ are 76.8, 66.5 and 58.7 wt% for SnO_2/C120-vap, SnO_2/C45-vap and SnO_2/C18-vap, respectively, which are very close to the W_{SnO2} determined by TG measurements (Table 1). This demonstrates almost perfect embedding of SnO_2 nanocrystallites in nanopores of porous carbons for SnO_2/C*X*-vap samples. On the other hand, agglomerated SnO_2 nanocrystallites were observed by TEM both in carbon nanopores and on the outer surface for SnO_2/C120-sol as shown in Fig. 1a. It can be concluded that *in situ* synthesis of SnO_2 with the introduction of vaporized Sn source is effective to deposit SnO_2 nanocrystallites dominantly in carbon nanospace.

Electrochemical measurements were carried out in a 1.0 mol dm^{-3} solution of $LiPF_6$ in ethylene carbonate/dimethyl carbonate against metallic Li at room temperature. A mixture of SnO_2/C*X* sample and poly(vinylidene difluoride) (PVdF) with the weight ratio of 90:10 were pressed on Ni mesh, and then were used as working electrodes. For the SnO_2 powder, 10 wt% of acetylene black (AB) was mixed as a conductive additive in the preparation of working electrode (See experimental details in ESI†). In the following, the SnO_2 electrode is denoted as SnO_2·AB. Fig. 2 shows cyclic voltammograms (CVs) of SnO_2·AB and SnO_2/C120-vap as representative examples. Redox peaks due to the SnO_2-Sn conversion reaction were observed around 1.2 and 0.9 V vs. Li/Li^+ in the cathodic sweep and around 1.1 and 1.9 V vs. Li/Li^+ in the anodic sweep. These peaks were remained on SnO_2/C120-vap even after 10th cycles in contrast that these peaks were almost disappeared for SnO_2·AB after the 2nd cycle, indicating that the reversibility of conversion reaction was improved for SnO_2/C120-vap. On the other hand, cathodic peak around 0.03 V and anodic peak around 0.6 V were ascribable to the redox of Sn-Li alloying and de-alloying reactions. The baseline current below 0.8 V was decreased and the change was almost saturated after the 2nd cycles, indicating that the alloying reaction at the initial cathodic sweep was accompanied with SEI formation. Because the redox peaks of alloying and de-alloying reactions for SnO_2/C120-vap were much larger and more stable than those for SnO_2·AB, the confinement of SnO_2 in carbon nanospace is also effective to enhance the reversibility of alloying

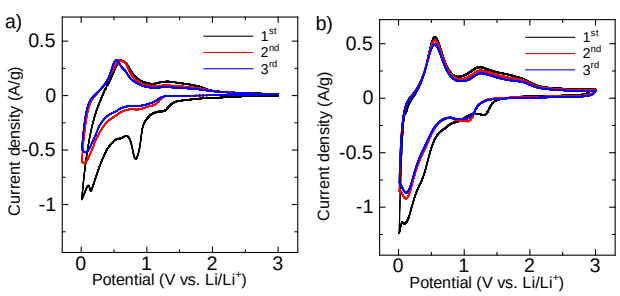

Fig. 2 Cyclic voltammograms of (a) SnO_2·AB and (b) SnO_2/C120-vap during 1st to 3rd cycles

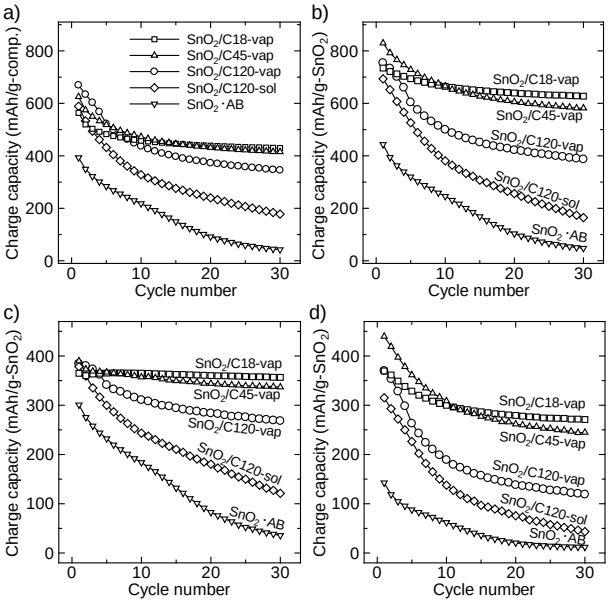

Fig. 3 Cycle performance in the potential range of (a, b) 0.01 to 2.0 V, (c) 0.01 to 0.9 V, and (d) 0.9 to 2.0 V. The charge capacities of (a) and (b-d) are based on the weight of composite materials and SnO_2, respectively.

and de-alloying reactions.

The charge-discharge properties were also evaluated by galvanostatic measurements. At the initial charge-discharge, the SnO_2/C120-vap showed higher capacity of the conversion reaction above 0.9 V than SnO_2/C120-sol and SnO_2·AB although charge capacities in the potential range of 0.01 to 0.9 V due to de-alloying were almost the same (Fig. S3, SEI†). As shown in Fig. 3a, the charge capacities based on the composite weight of SnO_2/C120 samples and SnO_2·AB were decreased with cycling the charge-discharge, but the SnO_2/C120-vap was superior in the capacity retention to SnO_2/C120-sol and SnO_2·AB. Fig. 3b shows the charge capacities based on SnO_2 weight which was estimated by subtracting the capacities of C*X*s measured at the same charge-discharge conditions (Fig. S4, SEI†). The same tendency as in Fig. 3a was confirmed on the SnO_2-based capacities for the three samples. These results indicate the confinement of SnO_2 nanocrystallites in carbon nanopores is effective to improve not only the capacity but also the cycle performance. The Coulombic efficiency with cycling and the rate capability were improved by embedding the SnO_2 in carbon nanopores, too (Fig. S5 and S6, SEI†). It was also found that the cycleablity was greatly enhanced with decreasing the pore size of C*X*s used for the synthesis of SnO_2/C*X*-vap samples. The SnO_2/C18-vap showed the highest cycleability among the SnO_2/C*X*-vap samples. The contribution of Sn-Li alloying and de-alloying reactions and SnO_2-Sn conversion reactions to the cycle performance was evaluated from these capacity retentions at the potential range of 0.01-0.9 V and 0.9-2.0 V, respectively (Fig. 3c, d). Surprisingly, the charge capacity retention of alloying reaction was almost constant around 100% for SnO_2/C18-vap during 30th cycling. On the other hand, the capacity retention of conversion reactions for SnO_2/C18-vap was 73.4% after 30 cycles, which is the highest value among those of SnO_2/C*X*-vap samples. These results clearly indicate that the reversibility of alloying and de-alloying reactions as well as conversion reactions can be enhanced by embedding SnO_2 nanocrystallites in the confined carbon nanospace. Consequently, SnO_2/C18-vap showed excellent total capacity retention of 85.4% after 30th cycles while keeping high capacities above 627 mAh g^{-1} of SnO_2, which is higher than or comparable to the best performance reported on nanocomposites of SnO_2 and carbon materials except for graphene materials.[14,16,23-26] The high capacity retention of SnO_2/C18-vap with cycling was preserved even after 100 cycles (Fig. S7, SEI†).

In conclusion, almost perfect embedding SnO_2 nanocrystallites into carbon nanopores were successfully achieved and the obtained nanocomposites showed excellent reversibility of Sn-Li alloying/de-alloying and SnO_2-Sn conversion reactions. The regulation of reaction field in confined carbon nanospace is one of the key to enhance the charge-discharge properties of SnO_2.

The study made use of XRD and TEM in the Center for Instruments Analysis of Nagasaki University. This work was partly supported by the Advanced Low Carbon Technology Research and Development Program of Japan Science and Technology Agency (JST) and a Grant-in-Aid for Scientific Research from Ministry of Education, Culture, Sports, Science and Technology of Japan.

Notes and references

Graduate School of Engineering, Nagasaki University, 1-14 Bunkyo-machi, Nagasaki 852-8521, JAPAN, E-mail: mrgch@nagasaki-u.ac.jp

† Electronic Supplementary Information (ESI) available: [Experimental details, XRD patterns of samples, SEM images of samples, initial charge-discharge curves of samples, charge-discharge properties of porous carbons, Coulombic efficiency, rate capability of samples, and cycle performance up to 100 cycles]. See DOI: 10.1039/b000000x/

1. Z. Junjie, Z. Lu, S. T. Aruna, A. Doron, A. Gedanken, *Chem. Mater.*, 2000, **12**, 2557.
2. K. Ui, S. Kawamura, N. Kumagai, *Electrochim. Acta*, 2012, **76**, 383.
3. L. Huang, H. B. Wei, F. S. Ke, J. S. Cai, X. Y. Fan, S. G. Sun, *Colloids Surfaces A Physicochem. Eng. Asp.*, 2007, **308**, 87.
4. H. Ahn, H. Choi, K. Park, S. Kim, Y. Sung, *J. Phys. Chem. B*, 2004, **108**, 9815.
5. C. Kim, M. Noh, M. Choi, J. Cho, B. Park, *Chem. Mater.*, 2005, **17**, 3297.
6. M.-S. Park, G.-X. Wang, Y.-M. Kang, D. Wexler, S.-X. Dou, H.-K. Liu, *Angew. Chem. Int. Ed. Engl.*, 2007, **46**, 750.
7. J. Ye, H. Zhang, R. Yang, X. Li, L. Qi, *Small*, 2010, **6**, 296.
8. Y. Wang, J. Y. Lee, H. C. Zeng, *Chem. Mater.*, 2005, **17**, 3899.
9. S. Ding, J. S. Chen, Q. Genggeng, X. Duan, Z. Wang, E. P. Giannelis, L. A. Archer, W. L. Xiong, *J. Am. Chem. Soc.*, 2011, **133**, 21.
10. X. W. Lou, Y. Wang, C. Yuan, J. Y. Lee, L. Archer, *Adv. Mater.*, 2006, **18**, 2325.
11. X. M. Yin, C. C. Li, M. Zhang, Q. Y. Hao, S. Liu, L. B. Chen, H. W. Tai, *J. Phys. Chem. C*, 2010, **114**, 8084–8088.
12. W.-S. Kim, Y. Hwa, J.-H. Jeun, H.-J. Sohn, S.-H. Hong, *J. Power Sources*, 2013, **225**, 108.
13. Z. Yu, S. Zhu, Y. Li, Q. Liu, C. Feng, D. Zhang, *Mater. Lett.*, 2011, **65**, 3072.
14. Y. Wang, F. Su, J. Y. Lee, X. S. Zhao, *Chem. Mater.*, 2006, **18**, 1347.
15. X. Chen, K. Kierzek, K. Wilgosz, J. Machnikowski, J. Gong, J. Feng, T. Tang, R. J. Kalenczuk, H. Chen, P. K. Chu, and E. Mijowska, *J. Power Sources*, 2012, **216**, 475.
16. P. Wu, N. Du, H. Zhang, J. Yu, D. Yang, *J. Phys. Chem. C*, 2010, **114**, 22535.
17. C. Feng, L. Li, Z. Guo, H. Li, *J. Alloys Compd.*, 2010, **504**, 457.
18. B. Zhang, B. Q. Zheng, D. Z. Huang, W. S. Oh, K. J. Kim, *Carbon*, 2011, **49**, 4524.
19. J. Cheng, H. Xin, H. Zheng, B. Wang, *J. Power Sources*, 2013, **232**, 152.

20. C. Zhang, X. Peng, Z. Guo, C. Cai, D. Wexler, S. Li, H. Liu, *Carbon*, 2012, **50**, 1897.
21. I. Moriguchi, F. Nakahara, H. Furukawa, H. Yamada, T. Kudo, *Electrochem. Solid-State Lett.*, 2004, **7**, A221.
22. *CRC Handbook of Chemistry and Physics*; Lide T. D. ed.; 75th edition; CRC press inc.: Boca Raton, 1994.
23. L. B. Chen, X. M. Yin, L. Mei, C. C. Li, D. N. Lei, M. Zhang, Q. H. Li, Z. Xu, C. M. Xu, T. H. Wang, *Nanotechnology*, 2012, **23**, 035402.
24. P. Wu, N. Du, H. Zhang, C. Zhai, D. Yang, *Appl. Mater. Interfaces*, 2011, **3**, 1946.
25. J. S. Chen, Y. L. Cheah, Y. T. Chen, N. Jayaprakash, S. Madhavi, Y. H. Yang, X. W. Lou, *J. Phys. Chem. C*, 2009, **113**, 20504.
26. Y. Lin, J. Duh, M. Hung, *J. Phys. Chem. C*, 2010, **114**, 13136.